




Applied Mathematics and Nonlinear Sciences

<https://www.sciendo.com>

Design Research of 600 M Scale Concrete Arch Bridge Based on Mathematical Optimization Method

Hongjiang Yu¹, Jiuqun Mao¹ , Qian Zhou², Boxu Cheng³, Xuesong Liu⁴, Chunlin Du⁵.¹Department of Traffic and Municipal Engineering, Chongqing Jianzhu College, Chongqing 400074, China²School of Urban Construction, Chongqing Nengyuan College, Chongqing 402260, China³Zunyi Traffic Survey and Design Co. Ltd. 563000, China⁴Chongqing Nanchuan Changda Jiaotong Investment Co., Ltd, Nanchuan 408400, China⁵Chongqing Municipal Design and Research Institute, Chongqing 400000, China

Submission Info

Communicated by Juan Luis García Guirao

Received January 14th 2020

Accepted February 22nd 2020

Available online august 27th 2020

Abstract

The mathematical algorithm of zero order optimization is a general function approach optimization method. Based on this method, many sets of analytical procedures are developed using ANSYS to study the design of 600m scale concrete arch bridge and the optimal arch axis coefficient, change mode and cross section sizes are obtained and verified. Results show: the mathematical algorithm of zero order optimization can effectively study the design of 600m arch bridge. The rich conclusions about design parameters can be a significant reference for design and further research of 600 m scale concrete arch bridge.

Keywords: The mathematical algorithm of zero order optimization; 600 m scale concrete arch bridge; optimal design; Arch axis coefficient; Section size

AMS 2010 codes: 90C31, 97R20

1 Introduction

The mathematical algorithm of zero order optimization is a general function approach optimization method, which is approximated by the least square method. Its essence is to find the extreme value of the function surface obtained to fit the solution space first. This mathematical algorithm is fast and can meet the calculation accuracy

[†]Corresponding author.

Email address: 674553405@qq.com

of most engineering requirements. No concrete arch bridge with a span of more than 600m has been built all over the world and special design guidance for this kind of super large span arch bridge is deficient.

Reinforced concrete arch bridge [1] has been favored by bridge designers worldwide due to its outstanding advantages of making full use of the mechanical properties of concrete and steel and owes a strong competitiveness among each kinds of arch bridges. Comparing with steel arch bridge and concrete filled steel tube arch bridge, the cost of concrete arch bridge with the same span is the lowest. In the past 20 years, the span of concrete arch bridge has been increasing rapidly and great progress has been achieved all over the world [2–8]. Among them, a series of researches on super long span concrete arch bridge were first conducted in Japan and Croatia [9]. But the first real concrete arch bridge with a span over 400m was the Wanzhou Yangtze River Bridge which was built in 1997 in china. Till today the Beipan River Bridge with a span of 445m on the Shanghai-Kunming High-Speed Railway in china which was constructed in 2016 has kept the world record for the span length of concrete bridges [10]. The large-scale construction of expressways and high-speed railways demands the development of long-span arch bridge, and advances in design and construction techniques and new materials such as high performance concrete [11] will make it possible to construct concrete arch bridges with a greater span in the future. Actually, concrete arch bridge with a span of more than 600 m is still in the research stage and a more rational structural design with good economic and safety performance is the first step to build these bridges.

Institute of civil engineering of Japan had tried out a trial design of 600 m scale concrete arch bridge in 1999, and the specification of “600m span grade concrete long arch bridge design and construction” was published in 2003. Among the scheme selections of Millau Viaduct Bridge which was built in France in 2004, a concrete arch bridge with a span of 602m was presented. A trial design of a arch bridge with a span of 600m was proposed in [12] and it was proved that concrete arch bridge was available to apply to the span of 600m. [13] proposed some measures to improve arch bridge’s mechanical performance in structure system and design parameters. [14] tried to conclude the evolution of design and construction techniques of arch bridge through three recent structures. China has begun to attach importance to 600m scale concrete arch bridge in recent 10 years, [15] introduced trial design of two foreign concrete arch bridges with a span of 600m and 602m to conclude some laws. [16]and [17] respectively studied on wind resistance performance and seismic performance of 600 m scale concrete arch bridge.

In fact, the larger the span of arch bridge, the higher requirements for safety and economy of structural design, a maximum reduction in cross section size to reduce dead load has become the primary concern of this kind of arch bridge. But there is little literature on this area at home and abroad. Cross section design of 600 m scale concrete arch bridge is studied deeply with arch axis coefficient, change mode and cross section sizes being investigated in this paper. Box section [18] is most suitable for super large span concrete arch ring with its advantages of light weight, strong bending resistance and torsion resistance, strong integrity and even force, and it is found that more than 80% of concrete arch bridges in China have adopted box section [19].

Based on the existing study results and optimization theory, the design of 600m scale concrete arch ring with box section is studied using multiple optimization method, optimal arch axis coefficient and change mode and cross section sizes for 600 m scale concrete arch bridge are obtained through a large number of optimization calculations with the large finite element software ANSYS. Furthermore, static, seismic and wind resistance [20] calculations on a design model built with these optimized data is conducted to verify its rationality. The presented conclusions can be a significant reference for design and further research of 600 m scale concrete arch bridge.

To promote the emerge of 600m scale concrete arch bridge, based on the mathematical algorithm of zero order optimization, many sets of analytical procedures are developed using the large finite element software ANSYS to study the design of 600m scale concrete arch bridge with box section.

2 Mathematical Algorithm Theory

2.1 Mathematical Method

Two mathematical optimization methods of zero order optimization and first order optimization are applied in ANSYS.

1) Zero order optimization theory

The zero order method, also known as direct method, uses only the dependent variable. It is a general function approach optimization method approximated by the least square method. Its essence is to find the extreme value of the function surface obtained to fit the solution space first. This method is universal in most engineering problems.

2) First order optimization theory

The first-order optimization algorithm uses the first-order partial derivative of the state variable and the objective function to the design variable. By adding a penalty function to the objective function, the constrained problem is transformed into an unconstrained problem. This method uses the derivative of objective function and penalty function of optimization variable to search in design space. The search direction is determined by gradient calculation, and the unconstrained problem is minimized by linear search method in the iteration.

The method of zero order optimization and first order optimization are most commonly used in engineering application. The zero order optimization method also called direct method uses least square method to obtain a function surface of which extreme value will be sought, and all constraints are approximated to the bounds in the iteration process. The first order optimization method is to transform the constraint problem into a non-constrained problem by adding a penalty function to the objective function, and the solution is searched by derivative of penalty function in the design space. The search direction is determined by gradient calculation, and the non-constrained problem is minimized by linear search method in iteration. This paper adopts zero order method as it is fast in calculating speed and can meet the accuracy requirements of engineering.

It is often need to minimize the weight, area, volume, stress and cost of the structure with the strength, rigidity, stability and dynamic performance of the structure meeting the safety requirements in engineering. This problem can be solved by optimization which is aiming to search the optimal values meeting the given requirements.

2.2 Mathematical Model

Design variables (DV), state variables (SV) and objective functions (OBJ) are used to describe the optimization process. Design variables are parameters that need to be continuously adjusted in the design process. State variables which can be functions of design variables or independent are the values of constraint design. Objective function is only related to the design variables and its extreme value is corresponding to the optimal design variables. The mathematical model can be expressed as follows:

$$\begin{aligned} \min f &= f(x) \\ g_i(x) &\leq 1.7Mpa \quad (i = 5) \\ w_{\text{lowerlimit}} &\leq w_i(x) \leq w_{\text{Upperlimit}} \quad (i = 8) \end{aligned} \quad (1)$$

Where: f denotes the objective function; w_i represent design variables and $w_{\text{lowerlimit}}$ and $w_{\text{Upperlimit}}$ respectively denote the given upper limit and lower limit; g_i represent state variables. Optimization design process in this paper is as shown in Fig. 1.

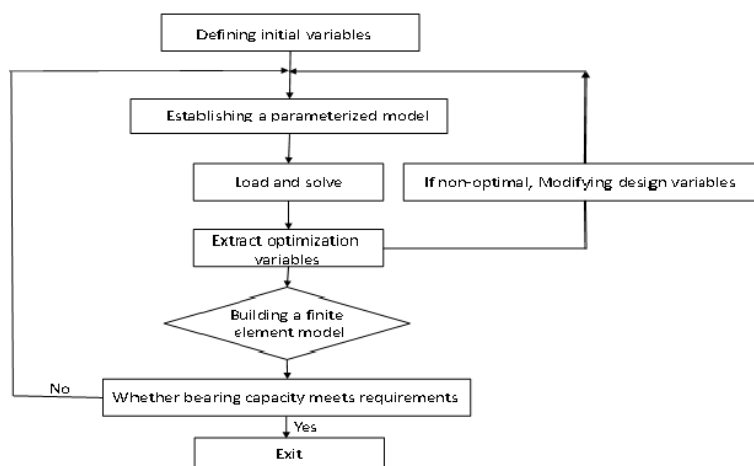


Fig. 1 Process of mathematical optimization

3 Trial Design of 600m Scale Concrete Arch Bridge

3.1 Investigation of Existing Design

Design value of buildings above the main arch ring, ratio of loss to span and distribution law of arch axis and their impact on the structure are learned on the basis of large number of existing research worldwide and the following conclusions are drawn: large span arch bridge had better choose catenary arch axis; the influence arch axis coefficient on bending moment is greater than that on axial force; the ratios of loss to span of the existing long-span concrete arch bridges are usually close to 1/6; the span of gastropore taking 40m is appropriate for 600 m scale concrete arch bridge; buildings above the main arch ring of super long span concrete arch bridge mainly include the type of continuous ventral hole, frame belly hole and continuous frame, among them, double column frame and T or box girder beam in steel-concrete composite form are respectively usually used for gastropore-piers and main girder.

3.2 Layout of the Trial Design

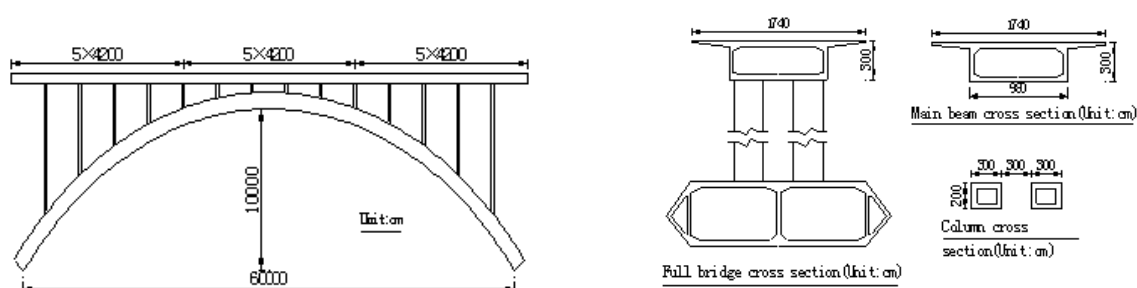


Fig. 2 Layout of the trial design

Based on the above conclusions and considering the fact that large span cable-stayed bridges and suspension bridges usually adopt flat section with wind fairing to increase wind resistance, catenary and hexagonal box section with wind fairing is adopted for the main arch ring in this paper. Layout of the trial design (Fig. 2) is determined referring to design and construction specifications of 600m long span concrete arch bridge in Japan. The girder chooses prestressed concrete rigid frame continuous beam with a span of 42m and a height of 3m,

the three spans near the vault adopt continuous beam and the rest adopt rigid frame to increase space between columns and to make construction convenient. Hollow thin-walled double columns is 3m in length, 2m in width and 0.45m in thickness.

3.3 Variable Section Model

There is little change in bending moment near mid-span position for hinged arch bridge and the form of variable cross sections are not fit, adopting a constant section for these positions will be more beneficial to improve mechanical performance and is more convenient for construction at the same time. In addition, with variable cross section at the two sides adopting construction method of cantilever casting and constant section in the middle part adopting construction method of stiffening skeleton, it is very suitable for this combined construction method which is usually adopted by large span arch bridges. The change mode mainly includes the two ways of changing width only and changing height and width at the same time for most of the existing long-span concrete arch bridges. For example, Miller viaduct in France adopts the former and the width is gradually changing from 8m to 18m. Institute of civil engineering of Japan choose the latter and the width and height are respectively changing from 23.5m to 11.5m and 10m to 6m. In this paper, the way of changing height and width at the same time is adopted for the trial design and the change mode of width is the same as that of a continuous rigid frame bridge which can be expressed as the following:

$$z = ax^N + c \quad (2)$$

Where: z denotes section width; x is horizontal distance from the section position to the foot; a and c are constants; N is variability index of width and z changes as a straight line when N takes 1.

3.4 Research status about cross section sizes for long span concrete arch bridge

The main dimensions of box section include: height(H), width(Z), roof and floor thickness(T_1) and web thickness(T_2). It is found that height of arch bridges with constant section and variable section are respectively $L/50$ - $L/90$ and $L/60$ - $L/90$ (L is span of arch bridge) according to large numbers of existing long-span concrete arch bridges. And the maximum height is 1.2-1.7 times of the minimum height for the variable section. In this paper, the height of the foot section chooses a small value of 10m and the height of the junctional cross section between variable part and equal part is 8.3m. They are accord with the design of Miller viaduct which is 8m in height and Institute of civil engineering of Japan which changes from 10m to 8m in height.

According to the specification of reinforced concrete arch bridge in China, the lateral stability should be calculated if width of the arch ring is less than 1/20 times of the span, according to it, width of the arch ring should have been over 30m for a arch bridge with a span of 600m. However, it has been found that width-span ratio can be reduced properly for super span concrete arch bridge. For example, width-span ratio of arch ring for main bridge and auxiliary bridge of KRK in Yugoslavia [22] are respectively 1/30 and 1/30.5, and that of Wan Zhou Yangtze River bridge in China is 1/26.25. the arch ring of Shibenik bridge in Yugoslavia adopts the minimum width-span ratio of 1/32.9 all over the world. Finally, the width of foot section and junctional section are respectively 24m and 14m in this paper.

The thickness of the box section is related to the span, load and mechanical property in the construction. It has found that thickness of roof and floor are generally 15-22cm and that of out and inside web is generally 15cm and 5cm-10cm for small span arch bridge; and it is found that the thickness increases greatly with the increase of span. For example, thickness of roof, floor and web of Fuling Wujiang bridge in Chongqing with a span of 200m and a form of single box with three chamber are all 20cm; and thickness of roof and floor is 40cm and that of web is 30cm for Wan Zhou Yangtze River bridge with a span of 420m and a form of single box with three chamber; thickness of roof and floor is 75cm and that of web is 50cm for the trial design advanced by Institute of civil engineering of Japan. In this paper, the thickness of roof and floor is 70cm and that of web is 50cm.

4 Optimization Research with Mathematical Algorithm

4.1 FEM Model

The main arch ring made of C80 concrete is simulated by shell63 element which has high calculate precision. With one unit being divided per 2m along the longitudinal direction, there are 7544 units for the whole arch ring. Diaphragms with a thickness of 30 cm are arranged at the columns, the middle position between two columns, the foot and the middle position between foot and the first column, and the diaphragms are also simulated by shell63 element. The spandrel column and deck made of C40 concrete are simulated by beam44 element. Mainly material parameters and FEM model are respectively as shown in Tab. 1 and Fig. 3.

The design variables (as shown in Fig. 4) and state variables [21] with their limit values in the following optimization model are respectively introduced in Tab. 2 and Tab. 3. The structure volume is usually taken as the objective function to reduce the structural weight, but this paper adopts the product of vault deformation and volume as objective function for the sake of taking mechanical property into account at the same time. The presented calculation results of the objective function are reduced by 1000 times in value to facilitate data statistics and analysis.

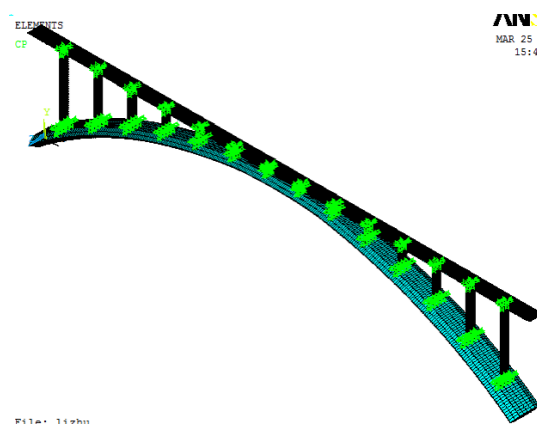


Fig. 3 FEM mode

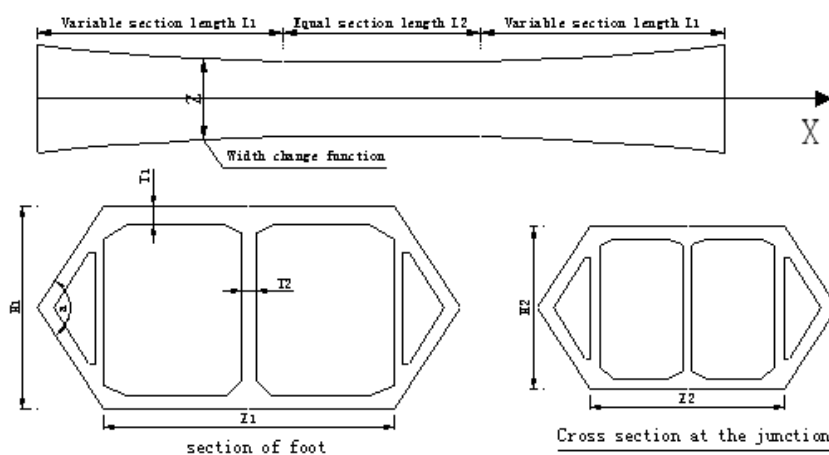


Fig. 4 Design variables

Table 1 Material parameters

Material	Modulus of elasticity/ (N/mm ²)	Mass density (kg/ m ³)	Coefficient of linear expansion	Poisson ratio
C80	3.80E10	2600	1.0E-5	0.2
C40	3.25E10	2500	1.0E-5	0.2

Table 2 Limits of design variables

Design variables	Symbol	Lower limit	Upper limit
Width of foot/m	Z1	15	25
Width of constant section/m	Z2	10	15
Height of foot/m	H1	8	15
Height of constant section/m	H2	6	10
variability index of width	N	0.5	5
Length of variable section/m	L1	100	300
Thickness of roof and floor/m	T1	0.4	0.6
Thickness of web/m	T2	0.4	0.6

Table 3 Limits of state variables

State variables	Symbol	Lower limit	Upper limit
Vault deformation/mm	DISP	-700	-400
First order elastic stability coefficient	FREQN	6	
Tensile stress of arch foot/MPa	SMAX1	0	1.7
Pressure stress of arch foot/MPa	SMAX2	-27	0
Tensile stress of L/8/ MPa	SMAX3	0	1.7
Pressure stress of L/8 / MPa	SMAX4	-27	0
Tensile stress of L/4/ MPa	SMAX5	0	1.7
Pressure stress of L/4/ MPa	SMAX6	-27	0
Tensile stress of L3/8/ MPa	SMAX7	0	1.7
Pressure stress of L3/8/ MPa	SMAX8	-27	0
Tensile stress of vault/MPa	SMAX9	0	1.7
Pressure stress of vault/MPa	SMAX10	-27	0

4.2 Optimization Research

4.2.1 Determination of Arch Axis Coefficient

The four cases with arch axis coefficient taking 1.6, 1.8, 2.0 and 2.2 are calculated to investigate its influence on the main arch.

At first, Z1, Z2, H1, H2, N and L1 are chosen as design variables with T1 and T2 being respectively assumed to be 0.5m and 0.55m in this section and the optimization results are shown in Tab. 4. It can be seen that with the increase of the coefficient of arch axis, the number of feasible solution increases and the impact the coefficient of arch axis on section sizes reduces. The range of design variables comes the largest meaning optimal space reaches the maximum when arch axis coefficient takes 2, and the structure tend to stable when the arch axis coefficient is over 2.

Then take L1 and N as design variables to conduct optimization to study the impact the coefficient of arch

axis on the form of variable section and the optimization results are arranged as shown in Tab. 5. Results show that L1, N, FREQN and the volume all decrease with the decrease of the arch axis coefficient, this is mainly due to the fact that the downward deformation of L/4 section increases with the decrease of arch axis coefficient, and in this case, L1 is decreased to increase downward deformation of the vault to meet the requirement of uniform deformation.

Finally take Z1, Z2, H1 and H2 as design variables to conduct optimization and the results are arranged as shown in Tab. 6. It can be seen that the volume reaches the minimum when the arch axis coefficient is 2.

To sum up, the arch axis coefficient taking 2 is rational for 600 m scale concrete arch bridge.

Table 4 Optimization results of arch axis coefficient

Number of solutions	4		3		7		13	
Arch axis coefficient	1.6		1.8		2		2.2	
Scope of solutions	lower limit	upper limit	lower limit	upper limit	lower limit	upper limit	lower limit	upper limit
Z1/m	22.12	23.68	19.40	21.05	17.19	23.48	17.90	23.48
Z2/m	10.14	11.75	10.02	10.15	10.02	13.00	10.02	13.00
L1/m	139.04	155.30	175.13	182.22	177.60	251.79	177.60	254.41
H1/m	12.72	13.30	13.59	13.81	10.24	15.00	10.24	15.00
H2/m	7.79	8.33	7.87	8.06	7.27	9.17	7.08	9.17

Table 5 Results of optimization

Arch axis coefficient	1.6	1.8	2	2.2
L1/m	137.84	163.33	180.98	217.00
N	3.39	3.60	3.83	4.80
Volume/m ³	14259	14698	14978	15622
FREQN	6.58	6.60	6.60	6.79
Vault deformation/mm	-398	-400	-417	-420

Table 6 Optimization results under different arch axis coefficient

Arch axis coefficient	1.6	1.8	2.0	2.20
FREQN	7.11	6.44	6.04	6.25
Vault deformation/mm	-401.67	-398.24	-429.90	-463.15
Z1/m	17.39	23.15	24.05	23.76
Z2/m	10.26	11.13	11.00	11.07
H1/m	14.90	12.91	12.86	12.65
H2/m	8.36	7.60	7.03	7.40
Volume/m ³	14462	14480	14014	14493

4.2.2 Optimization of Design Variables

According to multiple optimization method, firstly, overall optimization of all design variables on the above model with arch axis coefficient taking 2 is conducted based on zero order optimization method to find the preliminary range of feasible solutions, then every single design variable is optimized with random search approach to investigate the effect of each design variable on the objective function. The results of overall optimization are as shown in Tab. 7. Then choose L1 as the sole design variable with the others taking values of the sixth

Table 7 Results of overall optimization

Feasible solutions	1	2	3	4	5	6	7
L1(DV)/m	200.00	200.37	234.87	259.61	218.37	242.73	269.43
N(DV)/m	0.92	0.99	1.01	1.15	1.08	2.57	2.10
Z1(DV)/m	24.00	17.93	16.76	16.45	25.78	15.70	19.27
T1(DV)/m	0.60	0.58	0.51	0.51	0.55	0.47	0.54
T2(DV)/m	0.60	0.46	0.43	0.42	0.58	0.40	0.51
Z2(DV)/m	12.00	13.53	12.92	12.98	11.08	14.22	14.24
H1(DV)/m	14.00	12.51	14.51	14.85	13.47	11.59	10.02
H2(DV)/m	10.00	8.47	7.71	7.55	7.53	8.07	7.35
VOLUME(DV)	10.406	8.264	6.369	6.281	6.722	6.265	7.355
DISP(SV)/mm	-423	-487	-483	-475	-377	-533	-475

groups in Tab. 7 to conduct a series of optimal calculation and the optimum solution of L1 is achieved and can be plugged into the optimization calculation of the next design parameter. In this way, every design variable is determined one by one and the results are as shown in Tab. 8. Then the influence each feasible solution of design variables on objective function and all of the state variables is investigated and a large number of relation curves are achieved. Among them, the relationship between the feasible solution and the objective function (as shown in Fig. 5) and that between the tensile and compressive stress of the key section are given (as shown in Fig. 6 and Fig. 7) in this paper.

Table 8 The feasible solution of each design variable in local optimization

Feasible solution	1	2	3	4	5	6	7	8
L1(DV)/m	269.43	164.06	242.73	255.04	280.17	218.37	286.29	277.66
Z1(DV)/m	23.47	19.57	18.88	21.92	20.38	21.18	23.48	15.03
Z2(DV)/m	14.24	13.46	13.09	14.24	13.96	12.91	13.48	14.95
N1(DV)	3.96	2.10	1.86	2.92	2.38	2.66	3.47	0.51
H1(DV)/m	14.24	12.29	11.94	13.46	13.09	13.96	10.02	11.60
H2(DV)/m	9.24	7.29	6.94	8.46	7.69	8.09	9.24	8.96
T1(DV)/m	0.57	0.49	0.48	0.54	0.51	0.52	0.57	0.40
T2(DV)/m	0.57	0.54	0.49	0.57	0.56	0.54	0.42	0.60
feasible solution	9	10	11	12	13	14	15	16
L1(DV)/m	245.32	241.76	285.64	211.01	254.46	293.25	199.18	200.37
Z1(DV)/m	19.69	18.20	22.93	20.82	21.95	15.70	24.90	23.04
Z2(DV)/m	13.16	13.86	14.02	14.18	13.80	13.57	12.95	12.39
N1(DV)	2.14	1.62	2.54	3.27	0.75	0.89	1.03	3.00
H1(DV)/m	10.56	14.95	12.65	13.16	14.02	13.80	13.57	14.18
H2(DV)/m	9.24	7.29	6.94	8.46	7.69	8.09	9.24	8.96
T1(DV)/m	0.49	0.46	0.56	0.54	0.47	0.43	0.42	0.52
T2(DV)/m	0.55	0.56	0.57	0.54	0.55	0.41	0.52	0.42

(1) Optimization of L1

It can be seen from Fig. 4 that the object function decreases first and then increases with the increase of L1 and it keeps a small value when L1 changes from 220m to 280m; in addition, Fig. 6 and Fig. 7 show that the impact L1 makes on tensile or compressive stress of foot is greater than that on other sections, so the determination of L1 should be controlled by arch foot. It can be seen that the tensile and compressive stress of foot are basically stable and SMAX2 can meet the requirement of more than -27Mpa when L1 is larger than

220m. Therefore, L1 is finally taking the small value of 220m considering the construction convenience. At the same time, the range of L2 is 100m-200m(L/6-L/3).

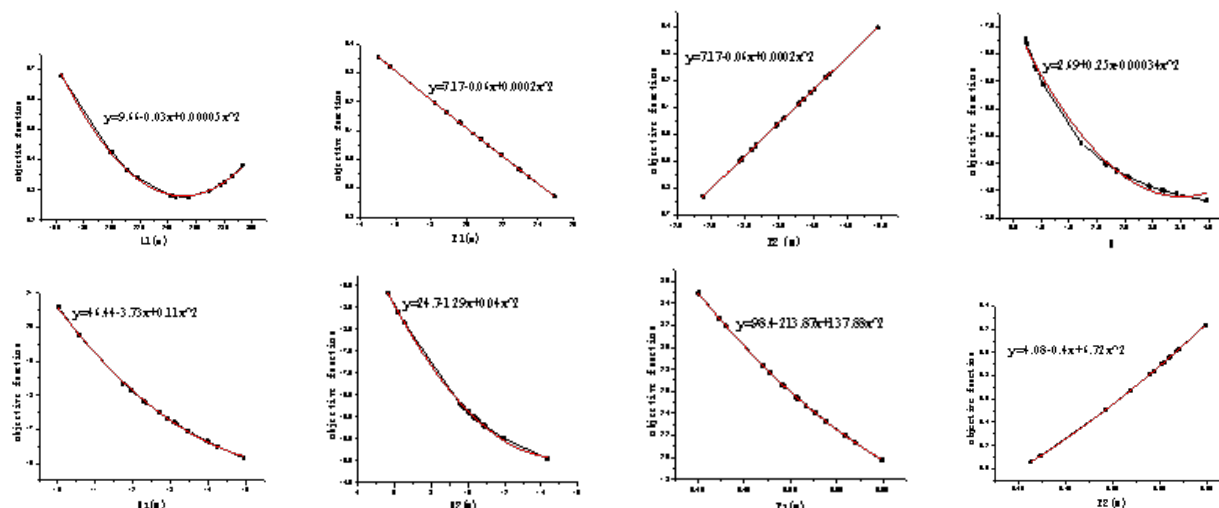


Fig. 5 Relation between feasible solution and objective function

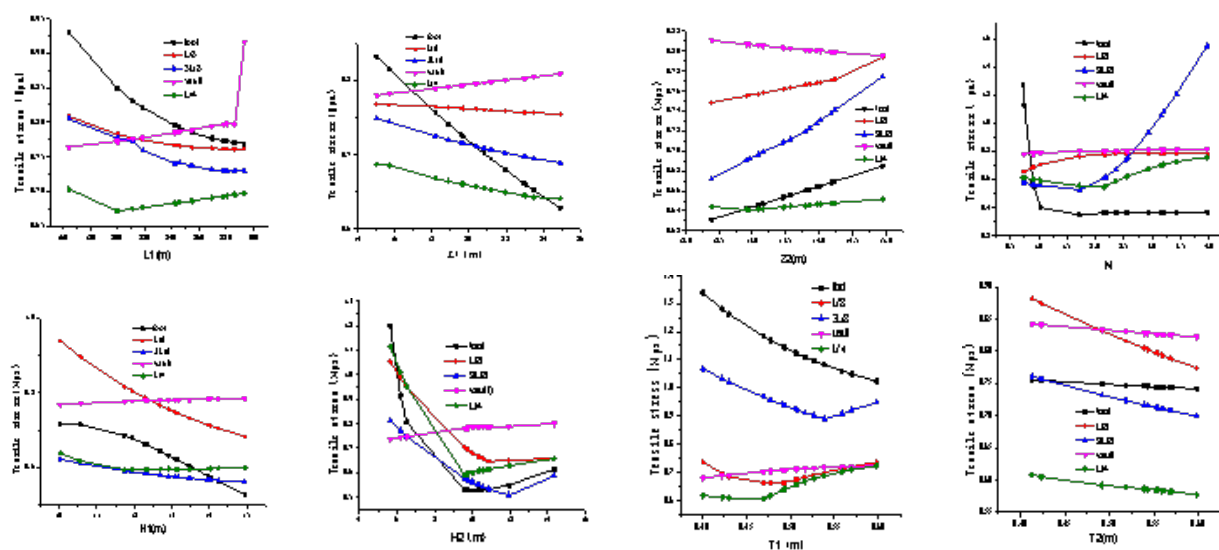


Fig. 6 Relationship between design variables and tensile stress

(2) Optimization of Z1

Z1 is optimized with L1 taking 220m and the others still taking values as the data of the sixth groups in Tab. 7. It is found that the larger the Z1, the smaller the object function; furthermore, Z1 is also controlled by the compressive stress of foot. As SMAX2 is less than -27Mpa when Z1 is larger than 22m, so the value of Z1 cannot exceed 22m.

(3) Optimization of Z2

Z2 is optimized with L1 and Z1 respectively taking 220m and 22m and the rest taking values as the data of the sixth groups in Tab. 7. Results show that the larger the Z2, the larger the object function; furthermore, the determination of Z2 is also controlled by the compressive stress of foot. As SMAX2 is more than -27Mpa when

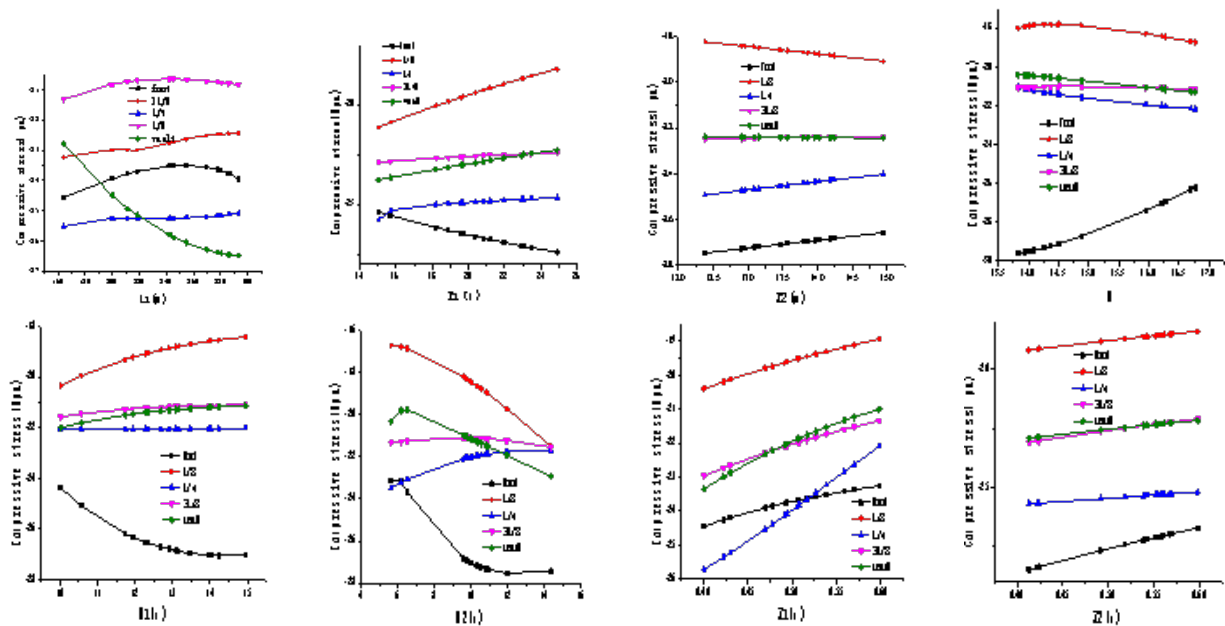


Fig. 7 Relationship between design variables and compressive stress

Z2 is larger than 13m, Z2 can take 13m in this paper.

(4) Optimization of N

It is found that N is mainly controlled by tensile stress of arch foot and it has great influence on the objective function when it is larger than 2; the tensile stress increases sharply with the decrease of N when N is smaller than 2, on the other hand, it will lost its practical application when N is larger than 3, so N can take values from 2 to 3.0 in engineering practice.

(5) Optimization of H1

It can be seen from Fig. 6 and Fig. 7 that H1 is mainly controlled by the compressive stress of the arch foot and is reasonable in the range of 12m 15m. It is suggested to take a large value of 15m to increase stability in this paper.

(6) Optimization of H2

H2 is respectively controlled by tensile stress and compressive stress of arch foot when it is larger than and less than 6.5m, As SMAX2 is more than -27Mpa when H2 is more than 7.5 m, this paper takes 7.5m.

(7) Optimization of T1

It can be found that the tension and compressive stress of the key sections can meet the given requirements for every feasible solution of T1, but FREQN is less than 6 when T1 is less than 0.42m. T1 can be in the range of 0.42m-0.6m in engineering practice.

(8) Optimization of T2

T2 is mainly controlled by the compressive stress of the arch foot and SMAX2 is more than -27Mpa when T2 is more than 0.55 m, so T2 should be more than 0.55m for this bridge.

In summary, the optimization results are concluded as shown in Tab. 9.

5 Verification of the Optimization Results

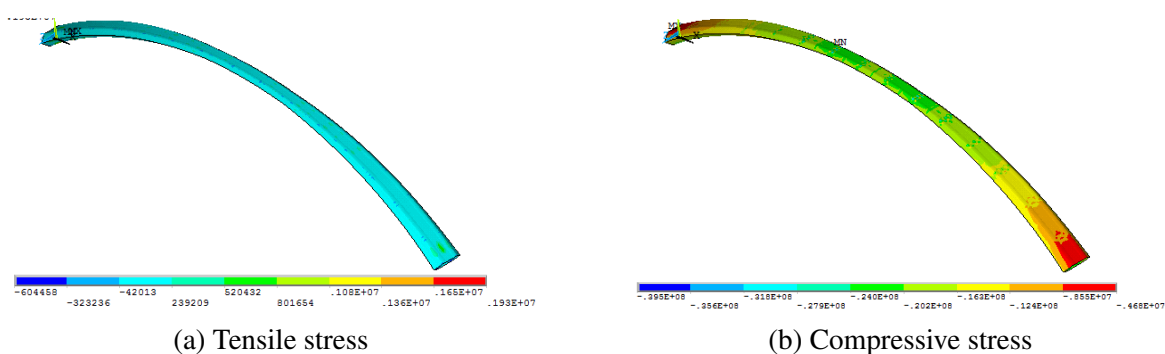
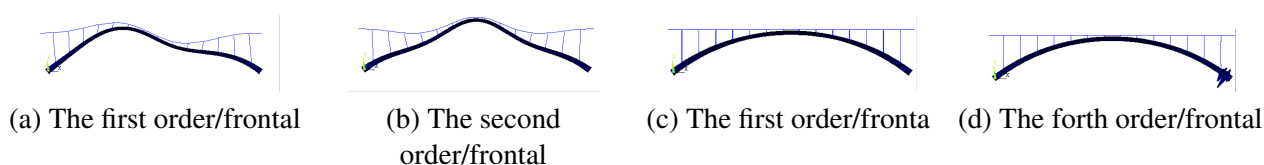
5.1 Static Analysis

The trial design with L1, Z1, Z2, N, H1, H2, T1 and T2 taking as the above optimum solutions is established and the results of static analysis are as shown in Fig. 8 and Fig. 9. It is found that the compressive stress

Table 9 Optimization results

Design variable	Symbol	Optimum solution	Feasible solution range
Width of foot/m	Z1	22	15-22
Width of constant section /m	Z2	13	13-15
Height of foot /m	H1	15	12-15
Height of constant section /m	H2	7.5	6-8
variability index of width	N	2.2	2-3
Length of variable section /m	L1	220	200-250
Thickness of roof and floor /m	T1	0.5	0.42-0.6
Thickness of web /m	T2	0.55	0.55-0.6

of the whole bridge is much smaller than the design value of C80 concrete and the maximum tensile stress being located at the bottom plate near the arch foot is 1.93MPa, and some pre-stressed steel bars are suggested to arrange at these location. Moreover, the stability coefficient of each order is more than the specification requirement of 4, the first and second order are in-plane instability which indicate that the external stiffness of the arch ring is large. Results show that strength and stability of the trial design can both meet the requirements.

**Fig. 8** Strength results under dead load**Fig. 9** Various buckling mode under dead load

5.2 Analysis of Seismic Behavior

(1) seismic vibration equation

The maximum earthquake force of a single point system can be expressed as the follows:

$$\begin{aligned}
 P &= C_z \times M \times \left| \ddot{\delta}_g + \ddot{\delta} \right|_{\max} = C_z \times M \times g \times \frac{\left| \ddot{\delta}_g \right|_{\max}}{g} \times \frac{\left| \ddot{\delta}_g + \ddot{\delta} \right|_{\max}}{\left| \ddot{\delta}_g \right|_{\max}} \\
 &= C_z \times k_H \times \beta \times G
 \end{aligned} \tag{3}$$

$$k_H = \frac{\left| \ddot{\delta}_g \right|_{\max}}{g} \tag{4}$$

$$\beta = \frac{\left| \ddot{\delta}_g + \ddot{\delta} \right|_{\max}}{\left| \ddot{\delta}_g \right|_{\max}} \quad (5)$$

The maximum earthquake force of multi particle system can be calculated as Eq. 6.

$$[M] \left\{ \ddot{\delta} \right\} + [C] \left\{ \dot{\delta} \right\} + [K] \left\{ \delta \right\} = -[M] \left\{ I_x \right\} \ddot{\delta}_g(t) \quad (6)$$

Where: g and G are respectively gravity acceleration and mass; k_H and β are horizontal seismic coefficient and dynamic expansion coefficient; C_z is influence coefficient of bridge ductility energy dissipation.

(2) Calculation results

Vibration frequency and mode are obtained first by modal analysis with subspace method [22] and are used to analyze the response spectrum combining with acceleration reflection spectrum. The mode participation coefficient is achieved through modal analysis using ANSYS as shown in Fig. 10. It is found that the mode participation coefficients in the three directions are all over 95% when the modal number is more than 150, therefore, the first 150 order seismic response spectra are taken to conduct calculation in this paper. Concrete shrinkage and creep are simulated by cooling 25°C on the arch ring since the span is too large. The strength results under seismic load are shown in Fig. 11.

Results show that: The maximum tensile stress of 1.93Mpa appears in base plate of arch ring near the arch foot and it is less than 1.31Mpa in other place, which meet design tensile strength requirement; the maximum compressive stress of the main arch is -28Mpa which is surplus comparing with the design value.

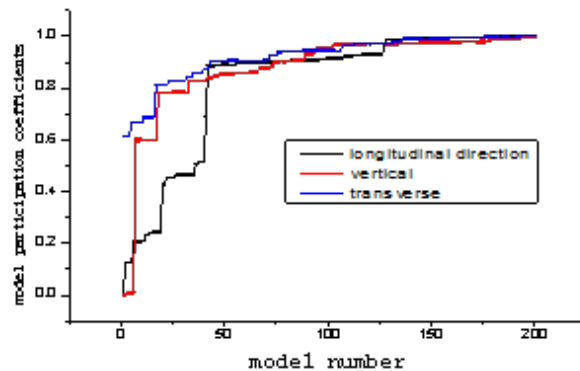


Fig. 10 Mass participation factor

5.3 Analysis of Wind Resistance

1) Calculation formula of wind load Design reference wind speed, static gust wind speed and lateral static gust load of bridge can respectively be calculated by Eq. 7, Eq. 8 and Eq. 9.

$$V_d = V_{S10} \left(\frac{Z}{10} \right)^\alpha \quad (7)$$

$$V_g = G_V V_d \quad (8)$$

$$F_H = \frac{1}{2} \rho V_g^2 C_H \quad (9)$$

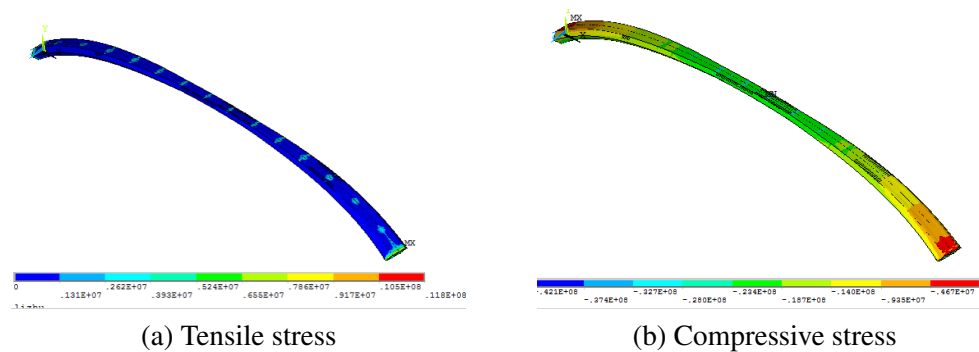


Fig. 11 Strength results under seismic load

Where: V_d , V_g and F_H respectively represent design reference wind speed, static gust wind speed and lateral static gust load; V_{S10} denotes design wind speed of the engineering site; Z , α , G_V , V_g and ρ respectively denote altitude height of structure, surface roughness coefficient, static gust coefficient, static gust wind speed and air density of the engineering site; C_H is resistance coefficient which can be calculated as follows:

$$C_H = \begin{cases} 2.1 - 0.1 \left(\frac{B}{H} \right) & (1 \leq \frac{B}{H} < 8) \\ 1.3 & (\frac{B}{H} \geq 8) \end{cases} \quad (10)$$

Where: B and H are width and height of cross section, respectively.

(2) Calculation results

Wind load are applied on the trial design the same as Lupu Bridge in Shanghai since they are close in span and loss (Fig. 12), and the fiducially wind speed, surface roughness coefficient, static gust coefficient and resistance coefficient of component respectively take 40 m/s, 0.16, 1.245 and 1.87. The calculation result of stability and strength under wind load and dead load are respectively given in Fig. 13.

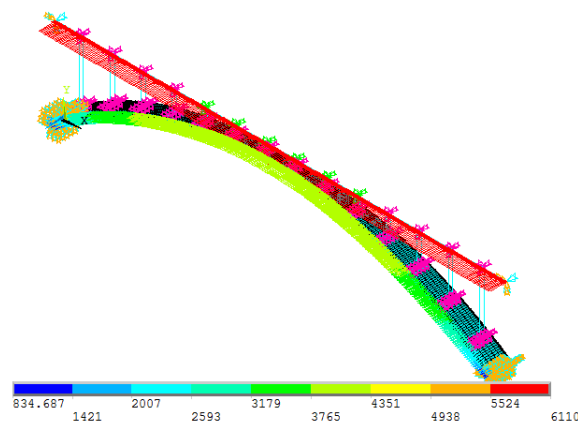


Fig. 12 Applied model of wind load

Results show that: the maximum tensile and compressive stress are respectively 2.07Mpa and -26.3Mpa under dead load and wind load; moreover, the first and the second order stability coefficient under dead load and wind load vary small compared with that under dead load only, but the stability coefficients of the third and the subsequent order reduce greater. This is due to the fact that the first and second order instability mode is in-plane instability which is little affected by wind load belonging to outside force. Therefore, there is small change in the stability factor of the first and second order.

To sum up, performance of static, seismic and wind resistance can all meet the design requirements, which

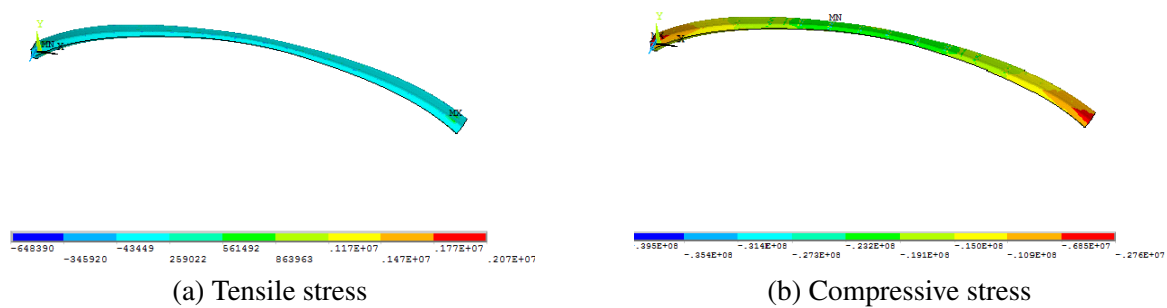


Fig. 13 Strength results under wind load and dead load

indicates that the trial design based on the optimization results is reasonable

6 Conclusions

The mathematical algorithm of zero order optimization is introduced in detail in this paper, and section design of the main arch ring for 600m span concrete arch bridge is studied with multiple optimization method which is the extension of zero order optimization. The following conclusions which can be a significant reference for design and further research of 600m scale concrete arch bridge could be drawn:

(1) The mathematical algorithm of zero order optimization can effectively study the design of 600m arch bridge, and the product of vault deformation and volume can be taken as the objective function, which takes stiffness and economy into account at the same time.

(2) It is reasonable to take 2 of the arch axis coefficient for 600m scale concrete arch bridge and the arch ring with a small arch axis coefficient will be prone to saddle deformation.

(3) The form of partial variable section at the two sides and constant section in the middle part is more advantageous than that of full variable section and the length for the middle part with a constant section is reasonable in $L/6$ $L/3$ (L is the span of arch ring); The change of width can adopt the model of polynomial with a variability index of 2.

(4) For super span concrete arch bridge, the width of the arch foot section and the constant section are respectively in the range of $L/40$ - $L/27.3$ and $L/46$ - $L/40$, and the height of the arch foot section and the constant section are respectively in the range of $L/50$ - $L/40$ and $L/100$ - $L/75$; the thickness of top and bottom flanges and that of web are respectively 0.42m - 0.6m and 0.55m - 0.6m.

(5) Calculation of static, seismic and wind resistance are carried out on the model established with these optimized data, and the results indicate that these optimization data based on the mathematical algorithm of zero order optimization is reasonable.

Acknowledgments

This research was funded by: Chongqing teaching committee science and technology project KJQN201805602; Chongqing Urban and Rural Construction Committee Construction Science and Technology Plan Project "Research Integration and Demonstration of Key Technologies in Assembled Housing Construction", Project No. 2015 (0-1); Intelligent Road Detection in Mountainous City Engineering Research Center of Chongqing Education Commission of China; Prefabricated Construction Applied Technology Promotion Center of Chongqing Higher Vocational Colleges.

References

- [1] Lu X, Lin K, Li C, et al. New analytical calculation models for compressive arch action in reinforced concrete structures. *Engineering Structures* 2018(168):721-735. doi.org/10.1016/j.engstruct.2018.04.097.
- [2] Bastidas-Arteaga E. Reliability of Reinforced Concrete Structures Subjected to Corrosion-Fatigue and Climate Change. *International Journal of Concrete Structures and Materials* 2018(12):1-13. doi.10.1186/s40069-018-0235-x.
- [3] Singh NK, Rai B. A Statistical Study to Investigate the Efficiency of Steel and Polypropylene Fiber in Enhancing the Durability Properties of Concrete Composites. *Civil Engineering Journal* 2018(06):1254-1270. doi.org/10.28991/cej-0309171.
- [4] Kang C, Schneider S, Wenner M, et al. Development of design and construction of high-speed railway bridges in Germany. *Engineering Structures* 2018(2): 184-196. doi.org/10.1016/j.engstruct.2018.02.059.
- [5] Zhou Q, Zhou SX, Li XQ, et al. Study on Construction Mechanical Properties of Cantilever-Pouring Concrete Arch Bridge. *Journal of chongqing jiaotong university (natural science)* 2018(7):9-18. doi.10.3969/j.issn.1674-0696.2018.07.02.
- [6] Moazam A, Hasani N, Yazdani M. Three-dimensional modelling for seismic assessment of plain concrete arch bridges. *Civil Engineering* 2018(3):1-36. doi.10.1680/jcien.17.00048.
- [7] Sun H, Zhu J, Ham S. Automated Acoustic Scanning System for Delamination Detection in Concrete Bridge Decks. *Journal of Bridge Engineering* 2018(6): 04018027-1-04018027-9. doi.10.1061/(ASCE)BE.1943-5592.0001237
- [8] Hiasa S, Birgul R, Matsumoto M, et al. Experimental and Numerical Studies for Suitable Infrared Thermography Implementation on Concrete Bridge Decks. *Measurement* 2018(121):144-159. doi.org/10.1016/j.measurement.2018.02.019.
- [9] Wei JG, Chen BC. Application and research progress of long span concrete arch bridges abroad. *World Bridge* 2009(2):4-8. 1671- 7767(2009)02- 0004- 05.
- [10] Zhang SY, Zhang RD, Jia Y, et al. Model Test Study on Long-Span Railway Concrete Arch Bridge with Rigid Skeleton. *Journal of Southwest Jiaotong University* 2017(6): 1088-1096. doi.10.3969/j.issn.0258-2724.2017.06.008.
- [11] Mészöly T, Randl N. Shear behavior of fiber-reinforced ultra-high performance concrete beams. *Engineering Structures* 2018(4):119-127. doi.org/10.1016/j.engstruct.2018.04.075.
- [12] Xie YZ. Structural Study of Arch Bridge with a Span of 600m Part I: Trial Design. *Applied Mechanics & Materials* 2011(138-139): 289-293. doi:/10.4028/www.scientific.net/AMM.138-139.289
- [13] Xie YZ. Structure Study of Arch Bridge with a Span of 600m Part II: Measures to Improve Mechanical Performance. *Applied Mechanics & Materials* 2012(138-139): 294-298. doi.10.4028/www.scientific.net/AMM.138-139.294.
- [14] Capellán G, Merino E, Sacristán M, et al. Recent Developments in Concrete Arch Bridges. *High Tech Concrete: Where Technology and Engineering Meet* 2018(298): 2621-2628. https://doi.org/10.1007/978-3-319-59471-2_298.
- [15] Cheng BC, Huang QW. Study on the test design of 600m span concrete arch bridge. *Chinese and foreign highway* 2006(1):80-82. 1671 -2579(2006)01 -0080 -03.
- [16] Xie CZ, Lin JQ. Analysis of Influencing Factors on Static Wind Stability of Super-large Span Reinforced Concrete Arch Bridge. *Western China Communication Science and Technology* 2017(6):88-91. doi.10.13282/j.cnki.wccst.2017.06.022
- [17] Fulin S , Airon L , Rui S , et al. Study of seismic performance of leaning-type arch bridge[C]// International Conference on Mechanic Automation and Control Engineering. IEEE, 2010.
- [18] Weiher H, Praus A, Runtemund K. Strengthening of 100 Year Old Concrete Arch Bridge “Kuhbrücke/Hildesheim”. *High Tech Concrete: Where Technology and Engineering Meet* (2018): 2004-2010. doi.org/10.1007/978-3-319-59471-2_229
- [19] Cheng BC, Wei JA, Zhou J, et al. Application of concrete-filled steel tube arch bridges in china:current status and prospects. *China civil engineering journal* 2017(6):50-61. doi.10.15951/j.tmgcxb.2017.06.006.
- [20] Hajali M, Jalali A, Maleki A. Effects of Near Fault and Far Fault Ground Motions on Nonlinear Dynamic Response and Seismic Improvement of Bridges. *Civil Engineering Journal* 2018(6): 1456-1466. doi.org/10.28991/cej-0309186.
- [21] Cao Y, Zhao N, Yu FR, et al. Optimization or Alignment: Secure Primary Transmission Assisted by Secondary Networks. *IEEE Journal on Selected Areas in Communications* 2018:1-1. doi.10.1109/JSAC.2018.2824360.
- [22] Chen YS, Lin YD. Novel subspace method for frequencies estimation of two sinusoids with applications to vital signals. *Iet Signal Processing* 2018(11): 1114-1121. doi.10.1049/iet-spr.2016.0702.